APPLICATION OF 3D CSAMT INVERSION TO VARIOUS DATA COMPONENTS AND ITS ENHANCEMENT

Ruizhong Jia and R.W. Groom, Petros Eikon Inc, Brampton, Canada

Abstract

We have developed a 3D inversion algorithm for CSAMT data incorporating a constrained trust-region technique. The algorithm is not limited by assumption regarding the farfield as we utilize a controlled source approach utilizing the specifics of the grounded transmitter incorporating not only the injected currents but also the induced fields from the transmitted magnetic fields. The inversion technique can be termed a quasi-Newton method with a fast convergence rate. The inversion algorithm can invert the electric fields, magnetic fields and/or impedance data to obtain a 3D resistivity distribution. We first utilize a synthetic example to demonstrate inverting the electric field data and impedance data. We have also studied enhancing the resolution of an inversion model when the strike and the dip of the structures is reasonably well known. In such a case, we discretize a 3D volume into grid cells which are oriented according to the known strike and dip angle. We have demonstrated that the inversion results can be dramatically improved by utilizing the dipping grid cells and imposing appropriate smoothing constraints along the dipping and strike direction. We also present various inversion results through inverting, separately and jointly, the impedance apparent resistivity and phase data. For the sake of a practical concern, we have focused on a case where the phase data are not reliable to be utilized in an inversion. Incorporating only the apparent resistivity data, our inversion results demonstrates that utilizing more frequencies may yield an improved inversion model.

Introduction

In this paper, we study aspects of our algorithm to invert various CSAMT data components. We utilize a constrained trust-region technique as the inversion method (Jia et al, 2009). This technique solves a least-squares minimization problem with simple bound constraints and has a fast rate of convergence. During the inversion process, we construct a quadratic approximation to the objective function utilizing a Taylor series expansion. In each iteration, a region around the iterate is defined by the trust-region radius. A quadratic model within this region is trusted to be an adequate representation of the objective function. The trust-region method then calculates the step to the approximate minimum of the model in this region. The direction and the length of the step are chosen simultaneously, as opposed to a line search strategy which chooses a search direction first and then focuses on finding a suitable length along this direction so that the objective function is approximately minimized. At each individual iteration, the trust radius is critical. If the radius is too small, the algorithm may not be able to take a substantial step to move closer to the minimum of the objective function. On the other hand, if the trust radius is too large, the model may not be an adequate representation of the objective function in the region specified by the trust radius. In such a case, we have to reduce the trust radius as the minimum of the model may be far from the minimum of the objective function in the region. We utilized a projected gradient method to determine an initial point with sufficient reduction of the quadratic model. The projected gradient method is more efficient as several bound constraints can be added simultaneously. As the second stage of the step computation, a further reduction of the quadratic model is sought to

enhance the convergence of the inversion with the additional restriction that the bounds on the parameters are kept fixed throughout the second process.

The forward simulation method incorporated in our inversion is based on the Localized Non-Linear (LN) approximator in (Habashy et al, 1993) and (Murray et al, 1999). This technique is efficient and stable in simulating three-dimensional electromagnetic scattering when scattering is controlled principally by either injected or induced currents in the host structures. It has proven useful in geological, near-surface environmental and geotechnical applications for almost 20 years.

Once a 3D inversion volume beneath a survey area is selected, we decompose it into *M* rectangular grid cells each of which has constant but unknown resistivity. The regular grid cells with zero dip angle are commonly utilized. However, in case of seeking a dipping structure, the grid cells with specified strike and dip angle are utilized to improve the inversion model resolution. The resistivity values of the *M* rectangular are expressed as a model vector, $\vec{K} = (k_1, k_2, \cdots, k_M)^T$. The LN forward modeling technique is utilized to compute the predicted data $\vec{d} = (d_1, d_2, \cdots, d_N)$. The measure of the data misfit is defined as $\phi_d = \left\| W_d(\vec{d} - \vec{d}_0) \right\|^2$, where $\vec{d}_0 = (d_1^0, d_2^0, \cdots, d_N^0)$ is the observed data, $W_d = diag(1/\sigma_1, 1/\sigma_2, \cdots, 1/\sigma_N)$, σ_i is the standard deviation of the *i*-th datum. The inversion model can then be determined by solving the minimization problem:

$$\text{minimize}\, \phi = \phi_d + \mu\phi_m,$$

where μ is a regularization parameter and ϕ_m is a model objective function that measures the smoothness of the resistivity distribution of an inversion model. The optimal value of μ will produce a data misfit equal to its expected value from the noise statistics.

We first use a synthetic example to demonstrate inverting the electric field data and impedance data. As inverting geological data for a dipping structure is a common and usually difficult task, we utilize a dipping slab-type conductive target. In cases where the strike and the dip angles of a linear structure are approximately known either by geology or gridding the data, we have investigated the possibility of enhancing resolution by incorporating such knowledge. Li and Oldenburg (2000), incorporate the known strike and dip angle information into the model objective function. In this paper, we demonstrate other ways to incorporate such known structural information. Specifically, we decompose a 3D volume into grid cells which are oriented along known strike and dip directions. There are two advantages of utilizing dipping grid cells. First, it is easier to impose smoothing constraints for the inverted models along strike and dip. It can also improve the recovered model resolution as a dipping linear structure can be better represented with the grid cells of the same orientation. We generated results by inverting first electric field data and then impedance data utilizing both a regular grid and a dipping grid. Our results demonstrated that an inverted model can be dramatically improved by utilizing the dipping grid cells and imposing appropriate smoothing constraints along the dip and strike direction.

When inverting CSAMT impedance data, we considered a commonly encountered difficulty: cases when the phase data were not accurate and reliable. In such a situation, only the apparent resistivity data can be utilized in the inversion. We conducted various inversions utilizing only the apparent resistivity data of our synthetic example. The results of inverting the apparent resistivity data at one particular frequency were not satisfactory. A joint inversion utilizing multiple frequencies yielded a much improved inversion model. This demonstrated the possibility of enhancing the inversion model resolution by incorporating more data components from multiple frequencies.

Synthetic Examples

To investigate inversion incorporating various data components, we construct a synthetic survey over an area of 2 km along the east-west direction and 1 km in the north-south direction (Figure 1). A slab-type anomaly was inserted into a uniform half-space with a resistivity of 1000 Ωm. The anomaly has a resistivity of 10 Ωm and is buried at a depth of 75 m to the top. It has a strike length of 1km, a dip extent of 500 m and a thickness of 10 m, striking along east-west direction and dipping 45 degrees to the south. Within the survey area are 11 north-south lines with a line spacing of 250 m. On each line there are 41 stations at intervals of 25 m. The lines are perpendicular to the strike direction of the anomaly.

A transmitter bipole source with a length of 2 km is oriented north-south and placed 3 km west of the center of the survey. The data of a magnetic field Hx directed east and an electric field Ey directed north were simulated as real and imaginary parts at 9 frequencies ranging from 1 Hz to 10 kHz. These simulated data were then contaminated with a noise of 2.5% of the datum magnitude. The impedance data were generated as $Z_{yx} = \frac{E_y}{H_x}$. The apparent resistivity was computed as in case of the simple plane wave, utilizing the relationship (Cagniard, 1953): $\rho_a = \frac{1}{\omega\mu}\left|Z_{yx}\right|^2$, where μ is the magnetic permeability of free space, ω is the angular frequency. The phase is $\phi = \arctan\left(\frac{im(Z_{yx})}{re(Z_{yx})}\right)$.

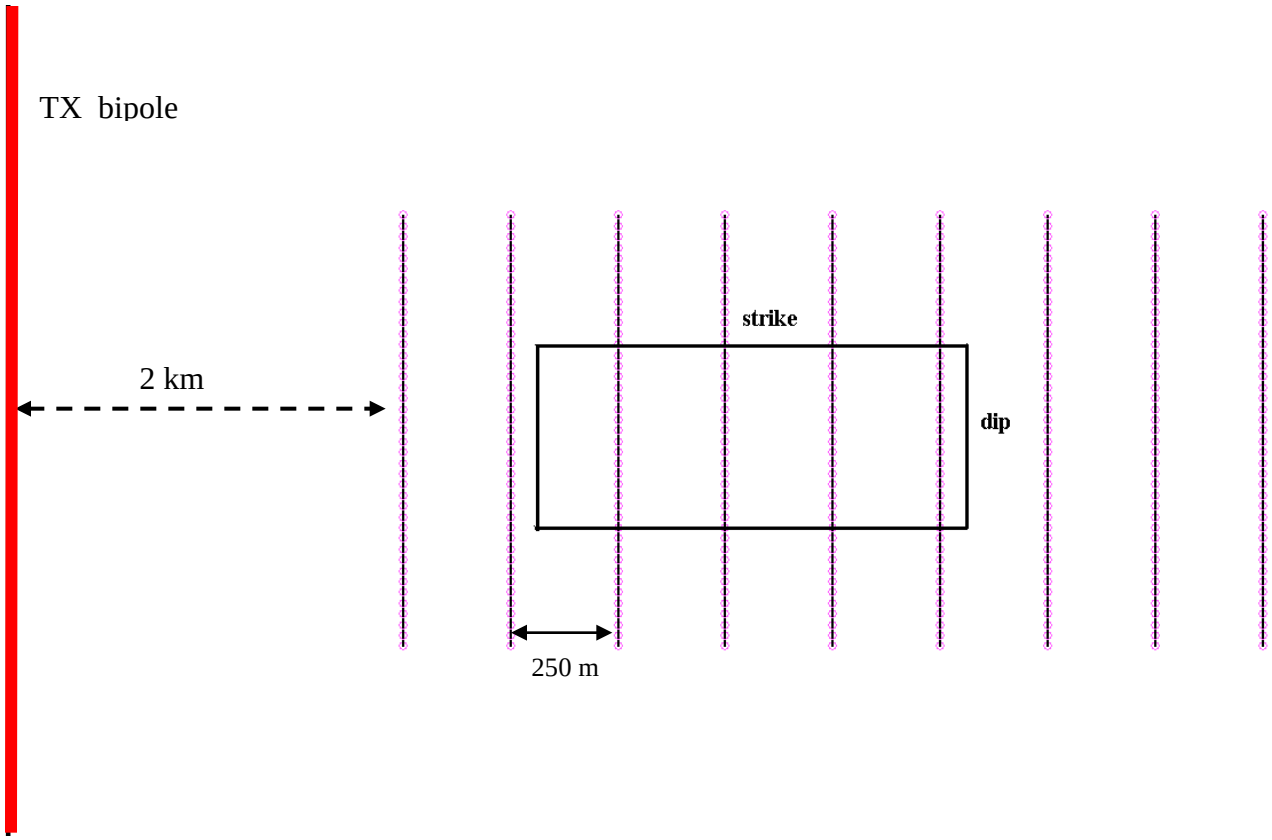

Figure 1: The plane view of the survey geometry and the dipping model in the synthetic survey. The red line on the left indicates the transmitter. The 4 black lines in the survey area represent the model.

Electric Field Data Inversion

We first inverted the real and imaginary parts of the electric field Ey of all the 9 frequencies utilizing a regular inversion grid. The 3D inversion volume has a dimension of 2200 x 1100 x 600 m and was discretized into 18x44 cells horizontally and 12 layers in the vertical direction. Each cell has a dimension of 125 x 25 x 50 m. The inversion begins with a uniform half-space with a resistivity equal to that of the true background (1000 Ωm). Assuming we know that the target is relatively conductive with respect to the background, the resistivity of the inversion grid cells was constrained between 1 and 1000 Ωm. We set the smoothing coefficients of the model objective function along the east-west, north-south and vertical direction to be (3, 0.1, 8), aiming at enhancing the smoothness of the inverted model in the vertical and the east-west direction.

Figure 2 is the north-south vertical slice of the inverted models through the center of the true model (x=-50). The black lines enclose the cross section of the true model. The conductive features in the inverted resistivity distribution models outline a dipping structure, although becoming smooth and broad at greater depths. Nevertheless, it provides a useful representation of the true model. The predicted data versus "true" data for 600 Hz are shown in Figure 3. Both the real and imaginary parts of the predicted data show a good agreement with the true data.

Inversion Utilizing A Dipping Grid

We now assume that the dip and strike angle of the target are known and demonstrate enhancements of the inversion by incorporating such information. We orientate the grid to the known strike (EW) and dip (45^o) utilizing the synthetic example presented above. Again a volume of 2200 x 1100 x 600 m was discretized with 18x32 cells horizontally and 17 layers vertically. Each grid cell has a length of 125 m, an extent down dip of 50 m and a thickness of 25 m. The starting model for the inversion is again a simply uniform half-space of 1000 Ωm and the resistivity of the cells is constrained between 1 and 1000 Ωm in the inversion. To strengthen the smoothness in the strike and dip directions, we imposed smoothness constraints in these directions with their coefficients being 3 and 8 respectively.

The predicted and *true* data for 600 Hz are shown in Figure 3 and a slice of the inverted model is displayed in Figure 4. By comparison with the regular grid inversion, it is seen that the inverted model with a dipping grid demonstrates a better recovery of the structure with higher resolution, particularly at depth. Both the predicted real and the imaginary parts agree well with the true data (Figure 3).

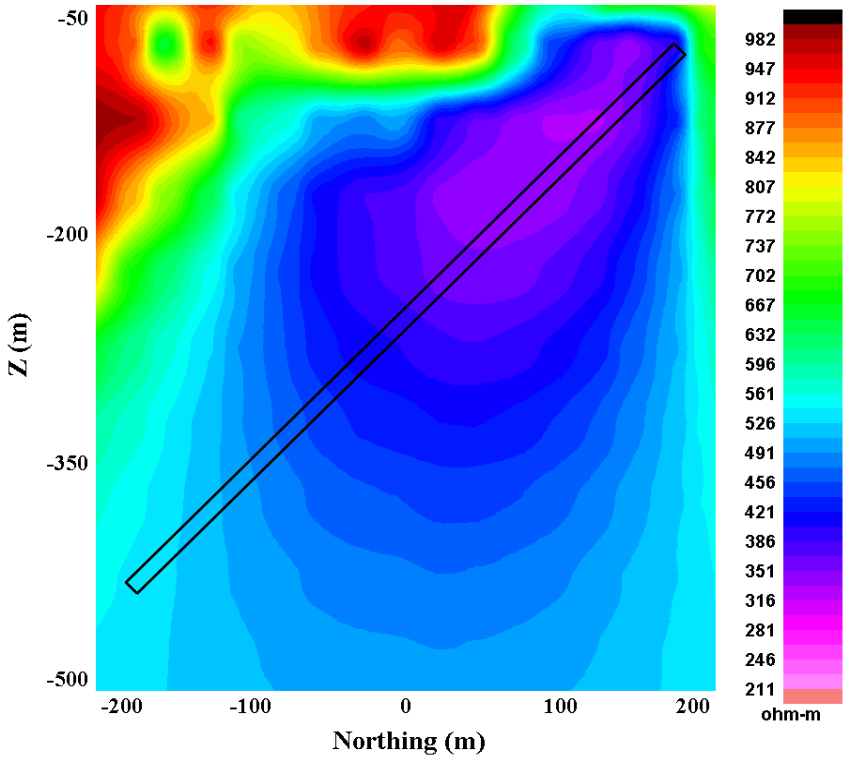

Figure 2: The inverted resistivity distribution model of Ey utilizing a regular grid. The north-south vertical slice of the inverted model through the center of the true model. The black lines enclose the cross section of the true model.

Impedance Data Inversion

We now illustrate the algorithm using the scalar impedance data. As with the electric field data inversion, the inversion volume had dimensions 2200 x 1100 x 600 m and was discretized into 18x44 cells horizontally and 12 layers in the vertically. The inversion starting model was a uniform half-space of 1000 Ωm and the resistivities of the cells were constrained between 1 and 1000 Ωm. The smoothing coefficients of the model objective function along the east-west, north-south and vertical direction were again set to be (3, 0.1, 8).

An inversion model slice is shown in Figure 5. The predicted versus true data at 600 Hz are displayed in Figure 6. Both the predicted apparent resistivity and phase agree well with the true data. The inverted model appears to show a dipping structure but loses resolution as the depth increases.

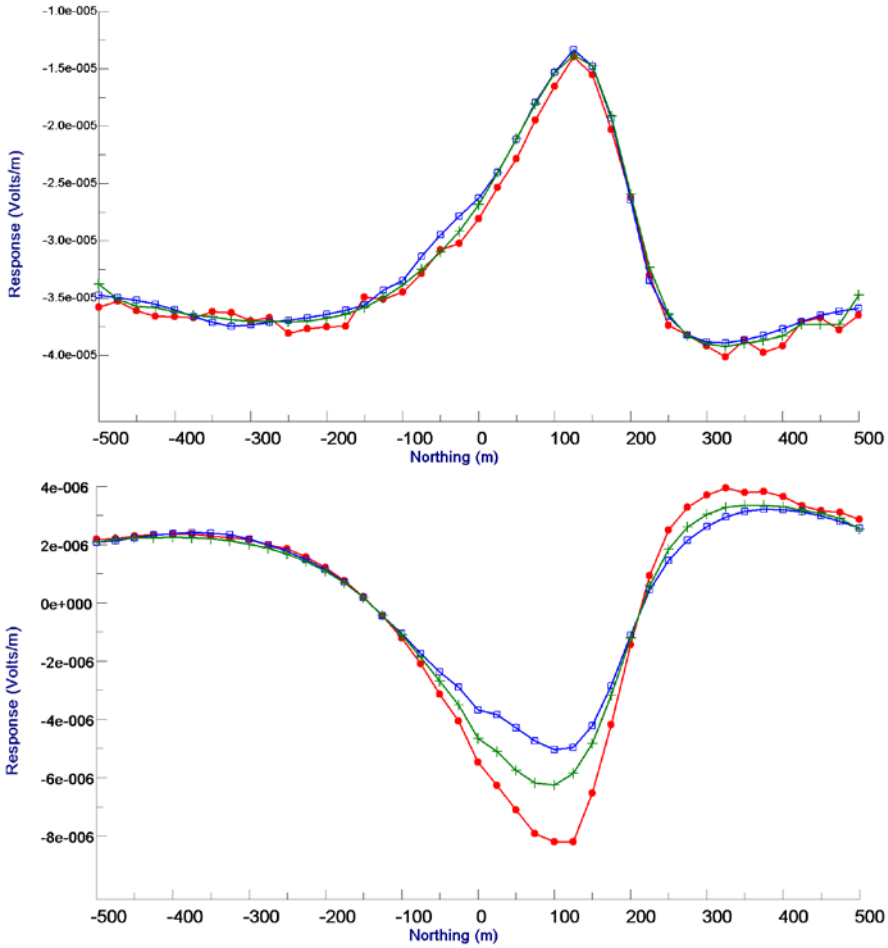

Figure 3: The electric field Ey at 600 Hz along the line over the center of the true model. The top plot is for the real part and the bottom one is for the imaginary part. The red curve represents the true data. The blue is the predicted data of the regular grid inversion. The green is the predicted data of the dipping grid inversion.

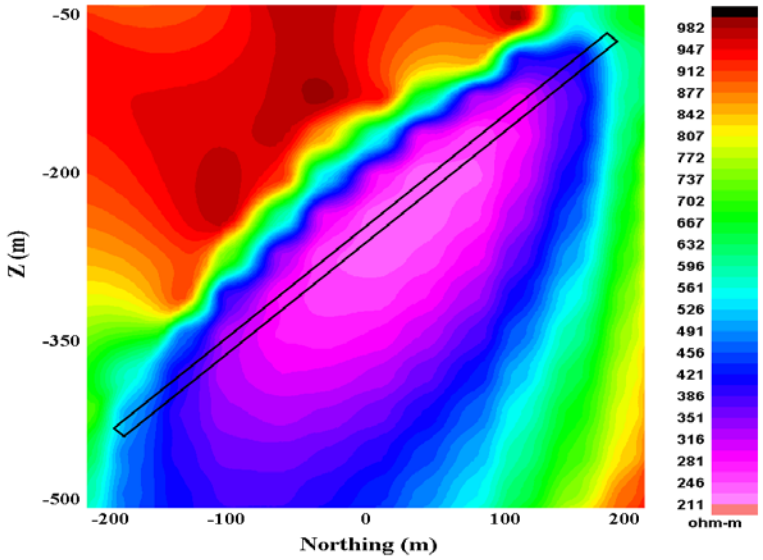

Figure 4: The inverted resistivity distribution model of Ey utilizing a dipping grid. The north-south vertical slice of the inverted model through the center of the true model. The black lines enclose the cross section of the true model.

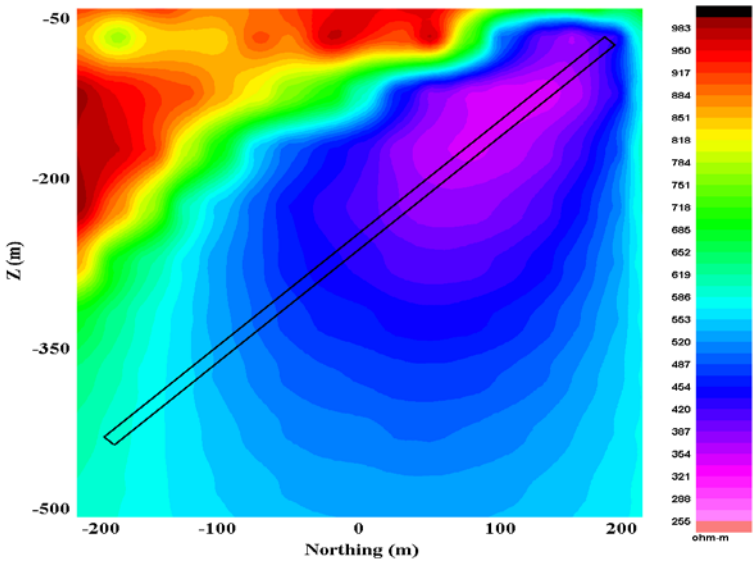

Figure 5: The inverted resistivity distribution model utilizing a regular grid and the resistivity data. The north-south vertical slice of the inverted model through the center of the true model. The black lines enclose the cross section of the true model.

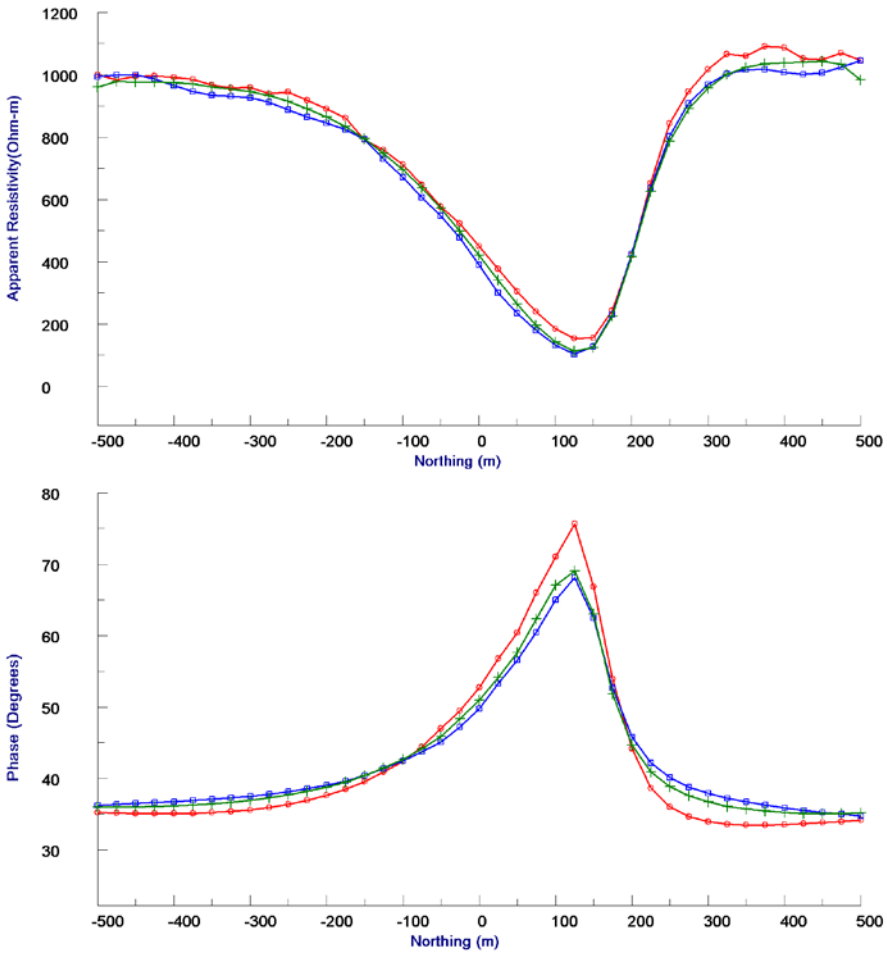

Figure 6: The impedance data at 600 Hz along the line over the center of the true model. The top plot is for the apparent resistivity and the bottom one is for the phase. The red curve represents the true data.

In this case, the impedance inversion for a regular grid is very close to the inversion results for the electric field alone. If we use the impedances with a dipping grid, the dipping grid impedance inversion is very close to the dipping grid electric field inversion. This is as expected. The resistivity of the background does not allow for significant induction of currents and so there are very small secondary magnetic fields although there may be large spatial variations in the magnetic field due to the 3D source.

However, one advantage of such an inversion approach is that should the magnetic field measurements be damaged in a survey, one could still apply inversion on the electric fields.

Conclusions

In the case that the strike and the dip angle of a structure of interest are known either by geology, gridding or simple modeling, we have demonstrated that the resolution of the inversion can be dramatically improved by utilizing dipping and striking grid cells with the known orientation. The resolution of the inverted results in the strike and dip directions can be easily controlled by the smoothing constraints in a model objective function and the structure can be better represented with grid

cells of the same orientation. The use of individual fields or the combined impedance ration provides more flexibility in structural determination as well as dealing with bad data.

References

[1] Cagniard, L., 1953, Basic theory of the magneto-telluric method of geophysical prospecting: Geophysics, 18, 605-635.

[2] Habashy, T. M., Groom, R. W. and Spies, B. R., 1993, Beyond the Born and Rytov Approximations: A Nonlinear Approach to Electromagnetic Scattering, Journal of Geophysical Research, 98, no. B2.

[3] Jia, R. J., Ruizhong, Davis, L. J. and Groom, R. W., 2009, Some issues on 1d-TEM inversion utilizing various multiple data strategies, SEG Expanded Abstracts, , 28: 739-743.

[4] Li, Yaoguo and Oldenburg, Douglas W., 2000, Incorporating geological dip information into geophysical inversions, Geophysics, Volume 65: 148-157.

[5] Murray , I. R., Alvarez , C. and Groom, R. W., 1999 Modelling of complex electromagnetic targets using advanced non-linear approximator techniques**,** Expanded Abstract, SEG.